OPEN

Citation: Cell Death and Disease (2017) 8, e2853; doi:10.1038/cddis.2017.247
Official journal of the Cell Death Differentiation Association

www.nature.com/cddis

Single-cell time-lapse imaging of intracellular O_2 in response to metabolic inhibition and mitochondrial cytochrome-*c* release

Heiko Düssmann[1,2], Sergio Perez-Alvarez[1,2], Ujval Anilkumar[1,2,3], Dmitri B Papkovsky[3,4] and Jochen HM Prehn*[,1,2]

The detection of intracellular molecular oxygen (O_2) levels is important for understanding cell physiology, cell death, and drug effects, and has recently been improved with the development of oxygen-sensitive probes that are compatible with live cell time-lapse microscopy. We here provide a protocol for the use of the nanoparticle probe MitoImage-MM2 to monitor intracellular oxygen levels by confocal microscopy under baseline conditions, in response to mitochondrial toxins, and following mitochondrial cytochrome-*c* release. We demonstrate that the MitoImage-MM2 probe, which embeds Pt(II)-5,10,15,20-tetrakis-(2,3,4,5,6–pentafluorophenyl)-porphyrin as oxygen sensor and poly(9,9-dioctylfluorene) as an O_2-independent component, enables quantitative, ratiometric time-lapse imaging of intracellular O_2. Multiplexing with tetra-methyl-rhodamine-methyl ester in HeLa cervical cancer cells showed significant increases in intracellular O_2 accompanied by strong mitochondrial depolarization when respiratory chain complexes III or IV were inhibited by Antimycin A or sodium azide, respectively, and when cells were maintained at 'physiological' tissue O_2 levels (5% O_2). Multiplexing also allowed us to monitor intracellular O_2 during the apoptotic signaling process of mitochondrial outer membrane permeabilization in HeLa expressing cytochrome-*c*-eGFP, and demonstrated that mitochondria post cytochrome-*c* release are able to retain their capacity to respire at physiological O_2 despite a decrease in mitochondrial membrane potential.

Cell Death and Disease (2017) **8,** e2853; doi:10.1038/cddis.2017.247; published online 1 June 2017

Aerobic organisms require a constant supply of molecular oxygen (O_2) to produce ATP through oxidative phosphorylation by mitochondria, a process that also leads to the formation of reactive oxygen species (ROS).[1] The response to O_2 levels in mammalian tissues is tightly regulated by specific genes and signaling pathways in order to maintain cell bioenergetics and survival.[2] Severe fluctuations in O_2 levels may lead to anoxia (no oxygen), hypoxia (decreased availability of O_2) or hyperoxia (increased O_2 levels), each condition capable of inducing cell and tissue damage. Because of uncontrolled cell proliferation, cancer cells are often exposed to tissue hypoxia. Many cancer cells are therefore specifically equipped to adapt and survive hypoxic periods.[3,4]

Similar to hypoxic conditions, mitochondrial cytochrome-*c* (cyt-*c*) release during apoptosis also induces a bioenergetics crisis, as cyt-*c* shuttles electrons between complexes III and IV.[5–7] Many cancer cells are resistant to caspase activation,[8] and when caspase activation is compromised, cancer cells may survive the bioenergetics crisis induced by cyt-*c* release, as the fraction of cyt-*c* remaining in the intermembrane space after equilibration with the cytosolic compartment may still be able to contribute to respiratory chain activity.[9–11] This enables mitochondria to sustain intracellular ATP in the absence of further mitochondrial degradation. This process is facilitated through enhanced extracellular glucose uptake, another key bioenergetics alteration of cancer cells.[9]

Because of the key role played by the mitochondrial respiratory chain in the control of cell survival during apoptosis, O_2 sensing represents an important method for the study of cancer energy metabolism and bioenergetics responses to metabolic inhibitors or mitochondrial cyt-*c* release.[12] Therefore, the development of new O_2 sensing and imaging protocols that enable measurements of oxygen levels in single living cells and during asynchronous, apoptotic cell death relative to other physiological parameters is of great interest to the cell death and bioenergetics community.

Significant progress has been made in the field of molecular O_2 detection by optical sensing.[13] The advantages of this technique are its sensitivity, accuracy and non-invasive nature.[14] Quenching of phosphorescence has become an important method for measuring O_2 by optical sensing.[15] Phosphorescence quenching relies on the ability of O_2 to quench the emission of excited triplet state molecules. In biological systems, phosphorescence quenching is highly specific to O_2, since oxygen is the only small molecule dynamic quencher present in sufficiently high concentrations.[16] Advantages of phosphorescent probes include high specificity, fast response, high sensitivity, stable calibration and various readout parameters such as intensity and lifetime. However, most of the probes developed still could not satisfy all the requirements for O_2 measurement in high-resolution imaging modalities in long-term experiments because of lack of

[1]Department of Physiology and Medical Physics, Royal College of Surgeons in Ireland, 123 St. Stephen's Green, Dublin 2, Ireland; [2]Centre for Systems Medicine, Royal College of Surgeons in Ireland, 123 St. Stephen's Green, Dublin 2, Ireland; [3]Luxcel Biosciences, Western Gateway Building, Cork, Ireland and [4]School of Biochemistry and Cell Biology, University College Cork, Cork, Ireland

*Corresponding author: JHM Prehn, Department of Physiology and Medical Physics, Royal College of Surgeons in Ireland, 123 St. Stephen's Green, Dublin 2, Ireland. Tel: +353 1 402 2255; Fax: +353 1 402 2447; E-mail: prehn@rcsi.ie

Received 09.12.16; revised 30.4.17; accepted 03.5.17; Edited by C Munoz-Pinedo.

compatibility with other probes, requirement of special imaging hardware, limited uptake into cells, or significant phototoxicity.[17] Detection techniques such as the Whalen-style platinum electrode[18] allow for the measurement of O_2 consumption at the single cell level,[19] but only deliver data for one cell at a time. Other optical intracellular oxygen sensing probes and techniques including Clark-type oxygen chips[20,21] often require highly specialized equipment such as fluorescence life time microscopy technologies.[21,22] As many laboratories routinely use confocal or epifluorescence time-lapse imaging, there is a significant need for the development of probes for these applications.[23,24]

In this study, we evaluated the utility of a nanoparticle-based phosphorescent probe, MitoImage-MM2, consisting of the O_2-sensitive phosphorescent reporter dye (PtTFPP) and the O_2-insensitive component (PFO) embedded in a cationic polymer,[25] for confocal time lapse imaging. We demonstrate that MM2 senses changes in oxygen concentration at single cell level in response to hypoxia, metabolic inhibitors and mitochondrial cytochrome-*c* release, and demonstrate its suitability for multiplexing with additional single cell fluorescent probes. Importantly, we also demonstrate that cell culture environment needs to be adjusted to more physiological conditions,[26] to more reliably detect alterations in cellular O_2 levels and mitochondrial bioenergetics.

Results

MM2 accurately measures O_2 concentration. The MM2 probe has been previously shown to be sensitive to O_2 and compatible with specialized detection platforms such as FLIM systems and time-resolved fluorescence (TR-F) readers.[25,27] Here we evaluated the capability of the ratiometric MM2 probe to monitor changes in O_2 concentration in HeLa cells loaded with MM2 nanoparticles, using a confocal live cell imaging setup. First, we explored the response of the probe alone under different O_2 concentrations. To this end we measured the MM2 ratio signal $R=(F_{PFO}/F_{PtTFPP})$ using 10 μg/ml of the probe in glass bottom cell culture dishes at varying O_2 concentrations on the live cell imaging setup, using the stage incubator described in Materials and Methods. In order to account for the variability of R ($t=0$ min) between experiments, we normalized R to its start value $R_0=R(20\%\ O_2)$. The on-stage calibration indicated a strong, linear correlation between the normalized MM2 intensity ratio R/R_0 and the oxygen concentration equilibrated to 20, 10, 5 and 2% O_2 (Figures 1a and b). The dependence of the PtTFPP intensity on the O_2 concentration is clearly visible in Figure 1a, while the PFO intensity remained stable during the calibration with 2, 5, 10 and 20% oxygen in the stage incubator atmosphere. Fitting to an exponential function provided the calibration equation $O_2\ [\mu M]=1/0.0045\ \exp\ (R/R_0/38.01)$, with an $r^2=0.9997$, representing an optimal fit. To confirm that the un-quenching of PtTFPP and therefore the drop in R/R_0 was reversible, O_2 in the buffer was again equilibrated to ambient O_2 at the end of each calibration experiment (Figures 1a and b).

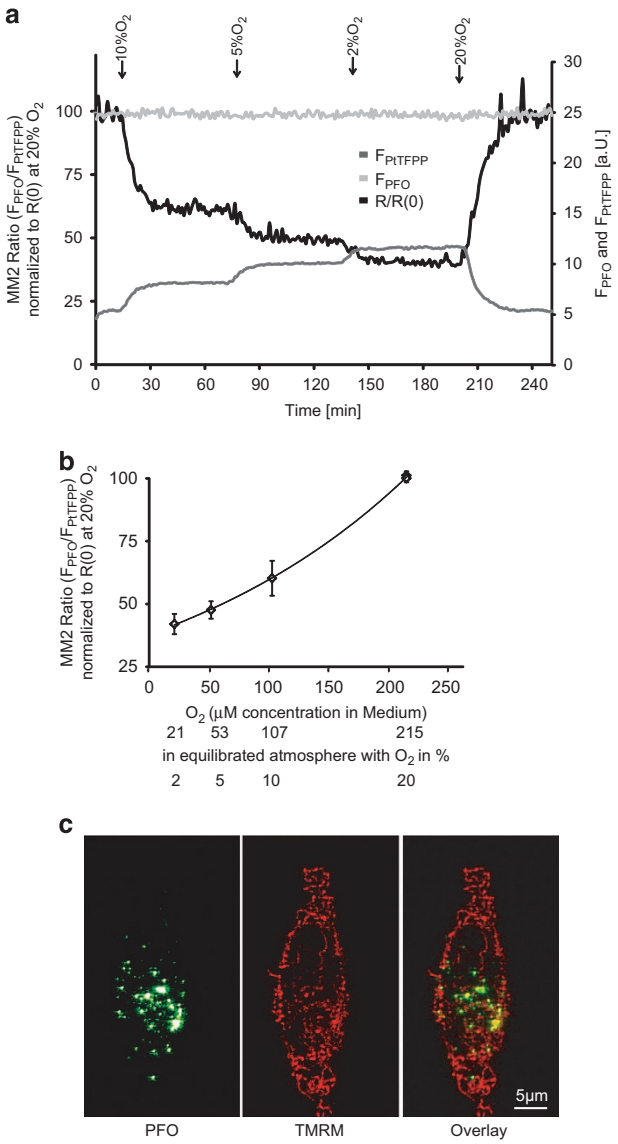

Figure 1 Performance of MM2 in ratiometric intensity-based oxygen sensing. (**a**) MM2 (10 μg/ml) was added to Willco dishes and covered with 1 ml mineral oil. Representative field of view-traces of fluorescence intensity ratio $R=F_{PFO}/F_{PtTFPP}$ normalized to R_0 for MM2 probe exposed to different oxygen concentrations (20, 10, 5 and 2% O_2). (**b**) Calibration curve resulting from measurements as in (**a**) for the MM2 fluorescence intensity ratio at indicated oxygen concentrations (215, 107, 53 and 21 μM O_2). Data are shown as $\pm$S.E.M. $^*p<0.05$ indicates difference between 225.74 μM O_2 at time point 0 min against different oxygen concentrations (215, 107, 53 and 21 μM O_2). Experiments were repeated three times on separate preparations with similar results. (**c**) Representative images showing uptake of the MM2 probe and mitochondrial TMRM in a HeLa cell. MM2 nanoparticles inside the cell, shown with one 1.2 μm thick optical section (FWHM, Scale bar, 5 μm)

MM2 is effectively loaded into HeLa cells. We next conducted a series of experiments to establish the best uptake conditions in HeLa cells. We incubated HeLa cells with 10 μg/ml MM2 probe in medium containing 10, 5, 2 and 1% of fetal bovine serum (FBS) for 16 h. This was required as the concentration of heat inactivated serum in the culture medium has been shown to affect the intracellular concentration of many probes and nanoparticles.[28] We identified 1%

FBS as the optimum condition to deliver the probe into the cells without affecting cell viability (data not shown). To investigate the distribution of the MM2 nanoparticles in cell culture, we obtained stacks of confocal images with an optical slice thickness of 1 μm of live HeLa cells incubated with the MM2 probe and 30 nM of the cationic dye TMRM, an indicator of mitochondrial membrane potential, ($\Delta\Psi_M$). Confocal analysis indicated that the MM2 signal derived from intracellular vesicles located in proximity to mitochondria (Figure 1c).

Effect of mitochondrial chain inhibitors on intracellular O_2 levels of HeLa cells maintained at 'supra-physiological' (20%) or 'physiological' (5%) ambient O_2. We next explored the effect of mitochondrial electron transport chain (ETC) inhibitors on intracellular oxygen levels and $\Delta\Psi_M$ as detected with TMRM. It has been shown that HeLa cells in a glucose-deprived medium shift their energy metabolism predominantly towards oxidative phosphorylation.[29] All experiments were therefore carried out with HeLa cells in glucose-free medium supplemented with 2 mM sodium pyruvate. HeLa cells loaded with MM2 probe and incubated with 30 nM TMRM were treated with ETC inhibitors, Antimycin A (AA; 10 μM), or NaN_3 (0.2 mg/ml). AA and NaN_3 inhibit complexes III and IV, respectively. As expected, inhibition of complex IV (Figures 2a and b) or complex III (Figures 2c and d) resulted in a significant decrease in the TMRM signal. Mitochondrial respiratory chain inhibition should lead to increased intracellular O_2 levels as oxygen consumption is strongly inhibited under these conditions. However only complex III inhibition induced a significant, detectable increase in intracellular O_2 when cells were maintained at 20% extracellular O_2 (corresponding to an extracellular O_2 concentration of 215 μM). The change of consumption after complex IV inhibition in medium equilibrated in 20% O_2 allowed us to determine the absolute intracellular concentration of O_2 in HeLa cells at the start of this experiment, assuming $R = R(20\%\ O_2)$ in cells treated with Antimycin A. Next we conducted a similar experiment, but reduced extracellular O_2 from 20 to 5% prior to complex inhibition to monitor responses at a more 'physiological' extracellular O_2 level occurring in normal tissues.[26] After 60 min of equilibration at 5% O_2, cells were exposed to AA (Figures 2g and h) or NaN_3 (Figures 2e and f). Reducing extracellular O_2 from 20 to 5% resulted in no significant decrease in TMRM average intensity, indicating that $\Delta\Psi_M$ was not compromised by this change. Under these conditions, addition of AA or NaN_3 induced a significant increase in intracellular O_2 concentration in response to ETC inhibition that was accompanied by a more pronounced drop in TMRM fluorescence intensity than in ambient O_2 (Figures 2e and f). Glucose oxidase and glucose was added at the end of the experiment to deplete all O_2 available in the medium, serving as an internal control for probe specificity to sense O_2.[27] Fercher and co-workers previously also showed that the respiratory capacity of cultured cells can be examined with mild stimulation of respiration by addition of low doses of a protonophore imaged with PtTFPP impregnated nanoparticles and phosphorescence life time imaging.[27]

Hypoxia limits consumption of O_2 in respiring HeLa cells with only a minor effect on $\Delta\Psi_M$. Next we analyzed the kinetics of $\Delta\Psi_M$ and O_2 consumption of respiring HeLa cells during incremental decreases of extracellular O_2. The O_2 concentration in the stage incubator was successively reduced from 20 to 10%, 5 and 2% O_2 which resulted in 215, 107, 53 and 21 μM dissolved O_2. O_2 levels were then returned to 20%. Again, we carried out the experiments in glucose-free medium supplemented with 2 mM sodium pyruvate, thereby forcing cells to use the ETC to fuel energy metabolism by consumption of O_2. The cells were stained with MM2 and TMRM. Interestingly, the change in the extracellular O_2 concentration from 5 to 2% still resulted in a significant decrease of available O_2 in HeLa cells without depleting intracellular oxygen completely (Figures 3a and b). $\Delta\Psi_M$ detected with the TMRM probe dropped stepwise with O_2 being reduced to 5% and then 2%, to significantly lower levels of $95.7 \pm 2.0\%$ (S.E.M.) and $85.7 \pm 2.2\%$ (S.E.M.) of the initial values. Interestingly, TMRM fluorescence intensity did not recover following the experiment and stayed at $80.9 \pm 3.6\%$ (S.E.M.) of the initial value, while O_2 returned to baseline levels (Figures 3a and b).

MitoImage-MM2 probe reveals respiration in single HeLa cells which underwent MOMP. We next explored whether multiplexing with the MM2 probe would also allow for simultaneous time lapse imaging of both cyt-*c*-eGFP redistribution and $\Delta\Psi_M$ using TMRM during apoptosis. Previous studies have suggested that oxidative phosphorylation activity and mitochondrial ATP production is still abundant after outer mitochondrial membrane permeabilization (MOMP) when caspase activation is compromised and glucose is available.[9,11,30] HeLa cells over expressing cyt-*c*-eGFP were pre-treated with 100 μM zVAD-fmk and then equilibrated at 2% O_2 for 60 min to mimic borderline normoxic/hypoxic conditions in tumors. Cells were then treated with the apoptosis-inducing broad-spectrum kinase inhibitor STS to induce the release of cyt-*c*-GFP. We hypothesized that a compromised ETC turnover after cyt-*c* release would cause an increase in intracellular O_2. Figure 4a depicts a representative image series, which demonstrates the successful multiplexing of MM2 with GFP and TMRM. Single cell cyt-*c*-GFP traces showed a significant decrease in the standard deviation of the pixel intensity of GFP fluorescence, indicating the onset of cyt-*c* release (Figure 4a, arrowheads in GFP channel indicate mitochondria before [323′] and after [326′] cyt-*c*-eGFP release; MOMP is indicated in Figure 4bi by filled arrowheads). The depolarization of $\Delta\Psi_M$ coincided with cyt-*c*-GFP release as reported previously,[9,31] but intracellular O_2 did not increase after MOMP in this cell, indicating that mitochondria were still consuming O_2. Once MOMP had occurred, we explored the effect of glucose addition on intracellular O_2 and $\Delta\Psi_M$. The addition of glucose recovered $\Delta\Psi_M$ in this cell (Figure 4a, TMRM; white arrowheads, before [380′] and after [420′] glucose addition). Of note, the addition of glucose also led to an increase in intracellular O_2 concentration in this cell, suggesting not only a decrease in F_oF_1-ATP synthase activity (indicated by increased TMRM fluorescence intensity), but also a concomitant decrease in ETC activity (Figure 4a, MM2,

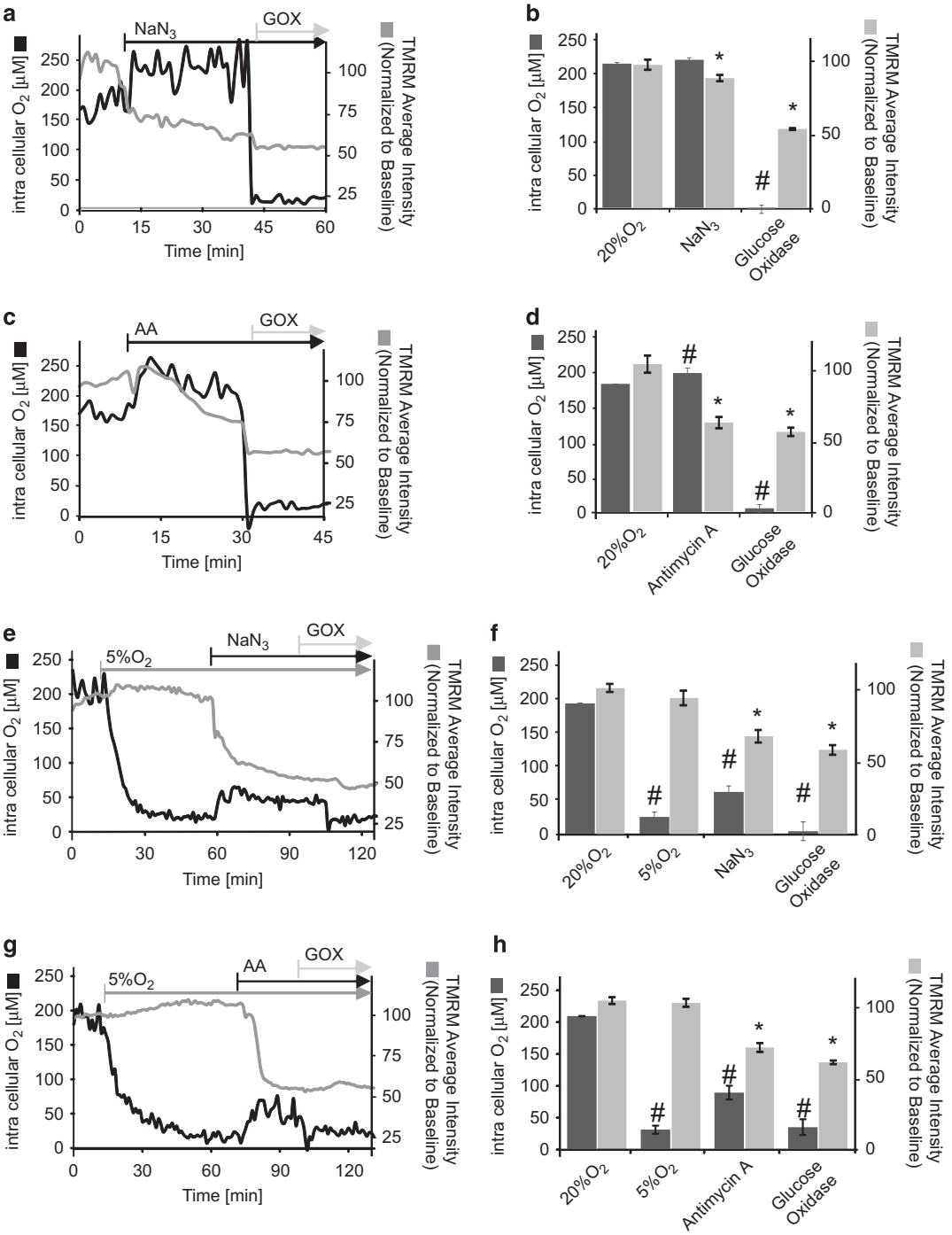

Figure 2 MM2 probe senses oxygen consumption by HeLa cells at 20 and 5% O_2. (**a**,**b**) Kinetics of MM2 probe intensity ratio in response to different electron transport chain inhibitors at the time points indicated at 20% O_2. HeLa cells were loaded with MM2 probe (10 μg/ml) and TMRM (30 nM) and mounted on a confocal microscope stage. Cells maintained at 20% O_2 and in medium without glucose supplemented with 10% FBS and 2 mM sodium pyruvate were exposed to Antimycin A (AA, 10 μM) (**a**) or NaN_3 (0.2 mg\ml) (**c**). Experiments were finished by addition of glucose oxidase (100 μg/ml). (**b**,**d)** Quantification of MM2 fluorescence intensity ratio at 20% O_2 and during the (**c**) AA or (**d**) NaN_3treatment. *and # indicate a significant difference with $p<0.05$, paired samples *t*-test, experiments were repeated two times on separate preparations. (**e**,**g)** Representative traces of changes in MM2 fluorescence intensity ratio following (**e**) AA (10 μM) or (**g**) NaN_3 (0.2 mg\ml) addition in cells maintained at 5% O_2. Cells incubated in medium without glucose supplemented with 10% FBS and 2 mM sodium pyruvate were maintained at 5% O_2 for 60 min to allow equilibration and then (**e**) AA or (**g**) NaN_3 was added to cells. Experiments were ended by addition of glucose oxidase (100 μg/ml). (**f**,**h)** Quantification of MM2 fluorescence intensity ratio at 5% O_2 and during (**f**) AA or (**h**) NaN_3. Data are shown as $\pm$S.E.M. *, $^{\#}p<0.05$, paired samples *t*-test indicates a significant difference between 5% O_2 in at 45 min against AA or NaN_3 treatment at 60 min, experiments were repeated three times on separate preparations

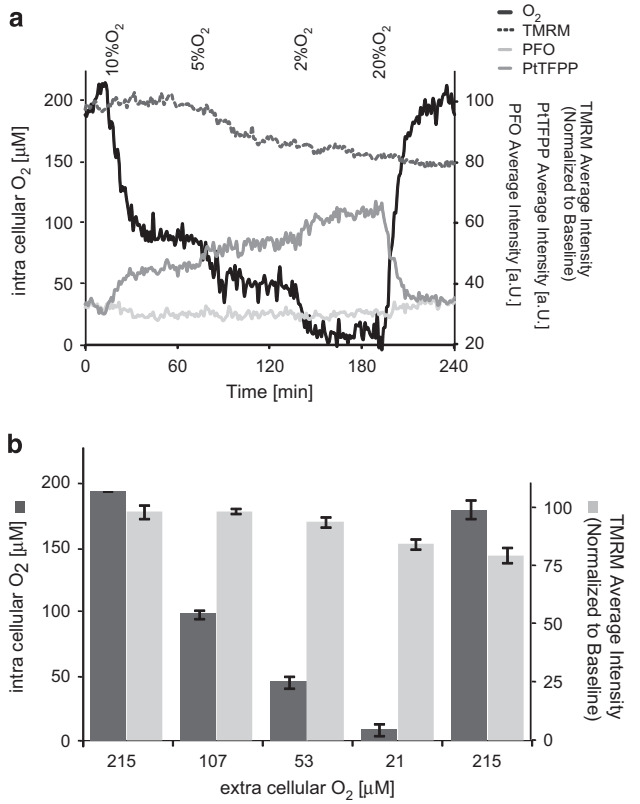

Figure 3 MM2 ratiometric intensity-based intracellular oxygen sensing within HeLa cells. (**a**) Representative kinetics of intracellular oxygen (black) and TMRM (black, punctate) average intensity one HeLa cell in the field of view in medium exposed to different oxygen concentrations equilibrating the medium to 20, 10, 5, 2 and back to 20% O_2. Single cell kinetics of PFO (light grey) and PtTFPP (dark grey) depict the stability of the PFO and the oxygen sensitivity of PtTFPP respectively. (**b**) Quantification of O_2 using the MM2 fluorescence intensity ratio at indicated extracellular oxygen concentrations. Data are shown as $\pm$S.D. of three independent experiments in HeLa

white arrow heads, before [380′] and after [420′] glucose addition). Hence MM2 can be used efficiently in multi-modal setup to measure O_2 concentrations in living cells without interference with GFP or green excitation/red emission probes such as TMRM.

By analyzing the single cell traces of $n=228$ cells that underwent MOMP during these experiments; we however also noted a significant heterogeneity in responses. MOMP resulted in an increase in respiration in 38 cells (decrease of intracellular O_2; represented by the single cell kinetics in Figure 4biii), in no change in 156 cells (as depicted in Figure 4bi), or a decrease in respiration in 35 cells (increase of intracellular O_2; represented by single cell kinetics in Figure 4bii). A quantification of these three types of responses is provided in Figure 4c. In order to investigate whether this was also determining the outcome of respiration changes after glucose addition, we separately analyzed the three response groups (Figure 4d). Interestingly, the majority of cells with a single-cell history of increased respiration after MOMP demonstrated decreased respiration after glucose addition. In contrast, cells which showed no response or a decrease in respiration after MOMP were less likely to decrease respiration after glucose addition. Furthermore, 149 of the 228 cells studied showed a recovery of $\Delta\Psi_M$ (as indicated by an increase of TMRM average intensity) after the addition of 25 mM glucose.

Discussion

In this report, we evaluated the potential of MitoImage-MM2 to probe alterations in intracellular O_2 levels and exploited the multiplexing capability of MM2. We found that exposure of HeLa cells loaded with MM2 to different oxygen levels accurately detected intracellular O_2 concentrations similar to *ex vivo* experiments. To explore whether MM2 reported alterations in O_2 levels as a consequence of changing mitochondrial respiration, we exposed HeLa cells to Antimycin A and NaN_3 and detected alterations in O_2 levels in particular when cells were maintained at more physiological tissue O_2 levels (2–5%). The complete O_2 consumption inhibition with NaN_3 enabled us to quantify the cellular O_2 concentration in cells kept in standard culture conditions. This then allowed us to calibrate single cell O_2 kinetics, and to simultaneously measure $\Delta\Psi_M$ kinetics.

MM2 is a second-generation probe for O_2 imaging, characterized by its PFO and PtTFPP, suitable for confocal and two-photon imaging.[25] In contrast to the loading of cells with nanoparticles incorporating PtTFPP alone,[27] MM2 can be used for ratiometric measurements. The dye combination used in MM2 also circumvents detector sensitivity issues with an emission wavelength above maximum at 650 nm,[32] making it suitable for confocal time lapse imaging.[33] MM2 was photostable with little bleaching and could be calibrated to estimate actual oxygen levels within cells. MM2 is compatible with fluorescent proteins, FITC- and rhodamine-based optical probes. Applications of second-generation phosphorescent probes for O_2 sensing adds speed,[19,34] and probes can be used for plate reader-based assays in parallel.[35] Interestingly, a cell-impermeable analog of MM2, PtP-C343, modified with polyethylene glycol residues, has recently also been shown to measure O_2 in brain microvessels when administered intravenously.[22]

Our confocal microscopy experiments indicated that MM2 was taken up and internalized in HeLa cells. While we have not yet defined the intracellular structures that incorporate MM2, a previous study using similar nanoparticles has identified uptake into endosomes in proximity to mitochondria.[27,36] Using the settings described in our study, we did not detect toxicity of the probe for up to 24 h after a 16-h incubation period, or phototoxic effects triggered by the image acquisition settings in control time lapse experiments. The detection principle used (quenching of the phosphorescence signal by O_2) will potentially generate ROS. To avoid this, acquisition settings have to be tested and adjusted to the highest sensitivity and lowest excitation light intensity and exposure time. This comes at the cost of increased noise, limiting the detection of subtle changes of intracellular O_2. However as we demonstrate in this report, MM2 is a highly interesting probe for detection of the kinetics of intracellular O_2 concentration by light microscopy, and enables the detection and classification of response types of intracellular O_2 changes even at low

atmospheric oxygen in multiplexing approaches at the single cell level as demonstrated in Figure 4.

Previous findings have shown that atmospheric O_2, cell density, respiration rate and its dynamics are the major factors influencing the oxygen-sensitive signaling pathways.[37] We show that alterations in oxygen levels in transformed HeLa cancer cells could be adequately detected at an oxygen level of 53 and even 215 μM (5% O_2 or 20% in the atmosphere with 5% CO_2). This represents O_2 levels higher than found in the human body, which ranges between 9 and 21 μM in healthy

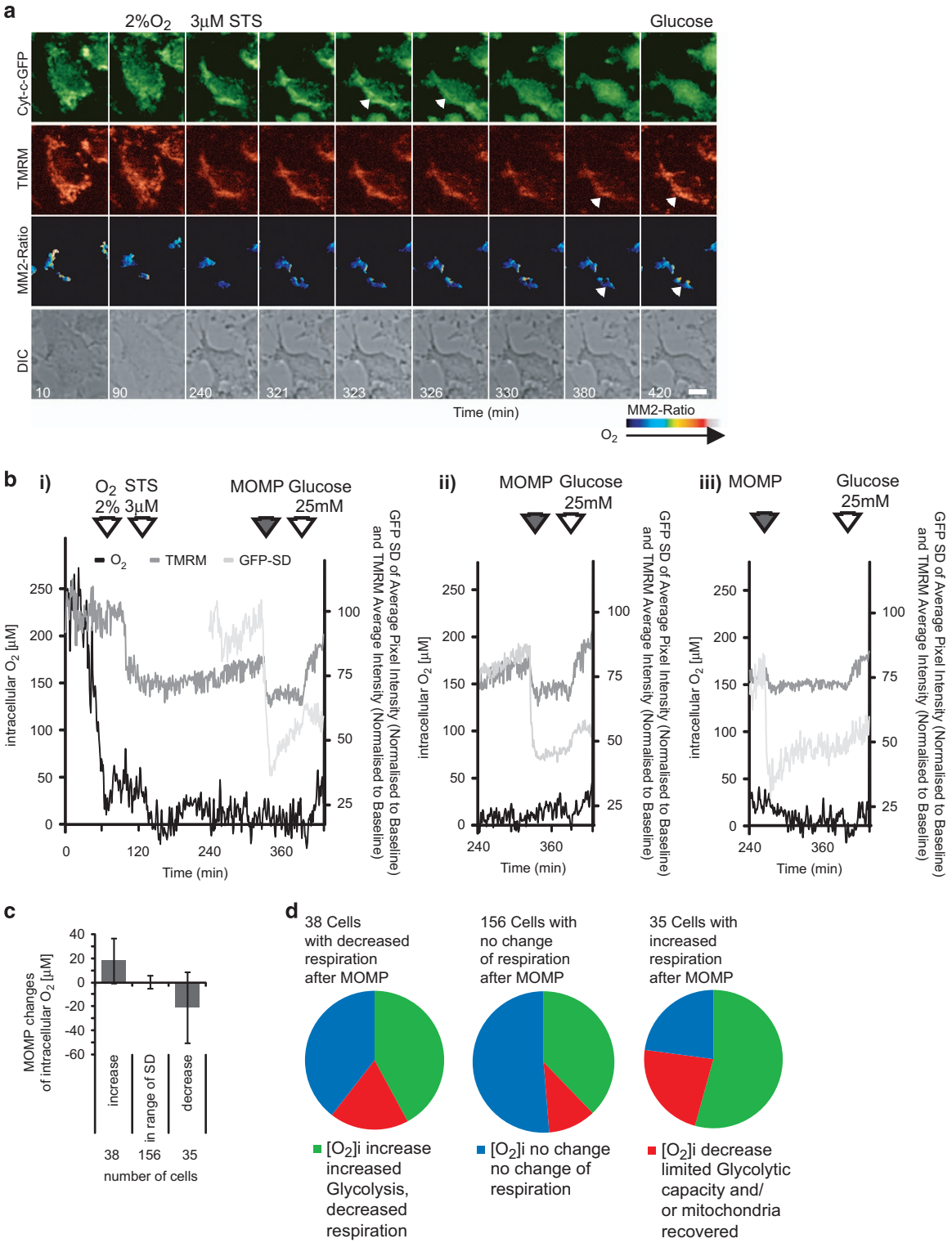

and 2.5and 13 μM in cancer tissue,[38] but still represents an extracellular O_2 level much lower than atmospheric oxygen (215 μM). At atmospheric O_2 levels, mitochondrial respiration inhibition with sodium azide did not induce significant alterations in intracellular oxygen levels. This may be due to the fact that dissolved O_2 at a high concentration (20%) can diffuse and equilibrate rapidly into the cells, rendering it difficult to detect changes in ETC O_2 consumption. Importantly, as oxygen consumption is central to ATP production via the respiratory chain, this implies that any analysis of cellular bioenergetics, such as mitochondrial membrane potential, ATP levels, ROS production, or NADH/NADPH levels should be performed under controlled oxygen levels.

Because mitochondria are the primary consumer of molecular O_2 and also control adaptive responses to hypoxia,[39–41] cellular O_2 levels can be an indicator of O_2-dependent metabolic activities, such as aerobic respiration or oxygen-dependent synthesis and degradation of cellular components,[33,42] and acts as a potential site for O_2 sensing in the cell.[43,44] Indeed, we found that simultaneously detected TMRM uptake to be different at 20 and 2% O_2 when cells fully rely on ETC to maintain their energy metabolism and fully depend on mitochondrial ATP. However, findings from isolated mitochondria suggest that mitochondrial O_2 availability does not become critically low and ATP production through ETC remains stable until the oxygen concentration falls near anoxic conditions ($<0.3\%$).[45,46] Tumor cells harbor the 'Warburg effect' which describes a switch from mitochondrial respiration to glycolysis in the presence of oxygen. However, recent studies have highlighted that this 'switch' is not complete and tumor cells are well capable of using mitochondria for aerobic ATP production.[47,48] Indeed, we show that inhibition of respiratory chain activity with Antimycin A or NaN_3 significantly increased intracellular O_2 in cells kept under physiological O_2 concentration.

Cytochrome-*c* is the main enzyme involved in transporting electrons and binds to oxygen in the ETC.[49] This, in turn, polarizes mitochondrial membrane potential, which drives proton motive force for ATP synthase to produce ATP.[50] In our experiments, cyt-*c* release during apoptosis depolarized $\Delta\Psi_M$ but had little effect on intracellular O_2 levels in the majority of cells, confirming previous reports that released cyt-*c* is still accessible for mitochondrial respiration.[11] Our study also demonstrates that, when glucose became available in cells which underwent MOMP, most cells responded with an increase in intracellular O_2, indicating that cancer cells are able to flexibly adapt to extracellular glucose increases post-MOMP with an increased glycolytic activity. Of note, our data also show a significant heterogeneity of bioenergetics responses post cyt-*c* release and glucose addition. This heterogeneity was not unexpected, as previous single cell imaging and mathematical modelling studies from our laboratory indicated a strong heterogeneity in mitochondrial respiration post MOMP, with cells operating different modes of complex V/ATP synthase activity in a given population of cancer cells, depending on the amount of respiration-accessible cyt-*c* and the degree of glycolytic ATP production.[9] This may also explain our findings that cells with increased respiration after MOMP (excessive respiration accessible cyt-c) were more likely to respond to an increase in extracellular glucose with a decrease in respiration, while cells with limited respiration (and limited accessible cyt-*c*) showed no decrease in respiration as a response to glucose addition.

The direct link between increased glycolytic activity and oxygen consumption in cancer cells that underwent MOMP may also be important in the context of ROS production and HIF-dependent and -independent hypoxia signaling, as both are strongly influenced by intracellular O_2 consumption and may control demise or recovery of cells post-MOMP.[51,52] The findings reported here may therefore also have important implications for tumor cell survival and resistance to therapy.

Materials and Methods

Materials. RPMI medium without glucose was from Gibco (Biosciences, Dublin, Ireland). RPMI medium, Antimycin A (AA), sodium azide (NaN_3), glucose oxidase from *Aspergillus niger* and carbonyl cyanide 4-(trifluoromethoxy) phenylhydrazone (FCCP) were purchased from Sigma Aldrich (Tallaght, Dublin, Ireland). Tetramethylrhodamine MethylEster (TMRM), fetal calf serum and Minimal Essential Medium were from Invitrogen (Biosciences, Dublin, Ireland). Staurosporine (STS) was from Axxora (Alpha technologies, Blessington, Ireland). Z-Val-Ala-Asp(O-methyl)-fluoromethylketon (zVAD-fmk) was obtained from Bachem (Heidelberg, Germany). The MitoImage-MM2 probe was provided by Luxcel Biosciences (Cork, Ireland).

Cell culture. HeLa cells and HeLa cells stably expressing cytochrome-*c*-eGFP (cyt-*c*-GFP,[31,53,54]) were grown in RPMI supplemented with 10% FBS at 37 °C in a humidified atmosphere at 5% CO_2. For the experiments, cells were seeded on glass-bottom culture dishes (WillCo Wells B.V., Amsterdam, The Netherlands), at a density of 20 000 per dish and maintained at 37 °C in a humidified atmosphere of

Figure 4 Multimodal imaging of MM2, cyt-*c*-GFP and TMRM at single cell level. Representative single-cell microscopic imaging of HeLa cells expressing cyt-*c*-GFP, loaded with MM2 (10 μg/ml) for 16 h, incubated with 30 nM TMRM, and caspase inhibitor zVAD-fmk (100 μM) 1 h prior to treatment with 3 μM staurosporine (STS, as indicated). The cells were kept in RPMI without glucose, supplemented with 10% FBS, and 2 mM sodium pyruvate. On stage the O_2 was maintained at 2% for 60 min before treating with STS. (**a)** Representative images of a single cell showing a decrease in TMRM after O_2 was downregulated from 20 to 2%, cyt-*c*-GFP release as an indicator for MOMP and subsequent further loss of TMRM, followed by recovery of TMRM after addition of 25 mM glucose to the cells (scale bar: 10 μm). The oxygen increase after addition of glucose is visible in the single (**b)** cell kinetics of that cell. The single kinetics of O_2 (solid black line), TMRM (solid dark grey) and SD of GFP average intensity (solid light grey, only displayed for significant time frame) show that the addition of glucose changes the intracellular oxygen level in the cell which underwent MOMP. The cell on the left (i) did not change respiration after MOMP as indicated by no change in intracellular O_2 while the cell represented in the middle (ii) showed an increase in intracellular O_2 indicative of a decrease in respiration. The cell represented by the kinetics on the right (iii) showed a decrease in intracellular O_2 indicative of an increase in respiration after MOMP. (**c)** Changes in intracellular oxygen concentration in cells undergoing MOMP. Out of 288 cells from 4 experiments, 255 cells showed a release of cyt-*c*-GFP (MOMP, indicated by grey arrowhead in **b**) after addition of STS and 228 before addition of glucose. Of those cells 38 showed increased oxygen concentration, 35 showed a decrease in and 156 showed no change in intracellular oxygen (data shown +/− S.D.). (**d**) Shows the three groups as separated in **c**. Glucose addition caused a heterogeneous response in respiration. A large fraction of all cells responded with a decrease in respiration. The single cell history with increased respiration after MOMP drove the majority towards a decrease of respiration after glucose addition. Cells which had no response or a decrease in respiration after MOMP were less likely to decrease respiration after glucose

5%CO_2/95% air. Experiments were carried out in glucose-free RPMI, supplemented with 10% FBS and 2 mM sodium pyruvate.

Monitoring changes in O_2 concentration using the ratiometricMM2 probe. HeLa cells were loaded with 10 μg/ml of MM2 (or co-loaded with TMRM for 30 min in the dark) in RPMI medium supplemented with 1% FBS medium for 16 h at 37 °C. MM2 probe intensity ratio was recorded at different oxygen concentrations (20, 10, 5 and 2% O_2) in a Willco dish mounted on LSM 5 live Duoscan confocal microscope (Carl Zeiss, Jena, Germany) equipped with a ×40, 1.3 NA Plan-Neofluar oil-immersion objective and a thermostatically regulated chamber (Pecon, Erbach, Germany) at 37 °C in a humidified atmosphere of 5% CO_2/95% air. $CO_2$and O_2 levels (%) in the stage incubator were regulated using the CTI controller 3700 Digital in combination with an O_2 controller (Pecon, Erbach, Germany). This unit requires N_2 to displace O_2 from the incubation atmosphere. The MM2 probe was excited using 2% of the 30 mW 405 nm DPSS Laser, and the emission was collected through a 415–480 nm band pass and a 570 nm long pass filter using a 565 nm secondary dichroic to split the emission between the two detectors of the LSM 5 live. TMRM was excited at 561 nm, and the emission was collected through a 570–640 nm band pass filter. In HeLa cells expressing cyt-*c*-GFP, GFP was excited with a 489 nm DPSS laser and the emission was detected using a 495–555 nm band pass filter. All images were processed using ImageJ (version 1.45, Wayne Rasband, NIH, Bethesda, MD, USA) and MetaMorph Software version 7.5 (Molecular Devices, Wokingham, Berkshire, UK). The intensity ratio images between the PFO and the PtTFPP (F_{PFO}/F_{PtTFPP}) were calculated for all areas of the image with PFO and PtTFPP fluorescence above background noise and after background subtraction. Mitochondrial membrane potential ($\Delta\Psi_m$) changes were measured using the average pixel intensity of TMRM per cell.

Sodium azide (NaN_3) and AntimycinA (AA) treatment at physiological (5%) and hyperoxic (20%) O_2. HeLa cells cultured on Willco dishes and incubated with the MM2 probe (10 μg/ml) for 16 h were co-loaded with TMRM (30 nM) at 37 °C in the dark for 30 min. The Willco dishes with cells were mounted on the stage of an LSM 5 live confocal microscope (Zeiss, Jena, Germany) equipped with a ×40, 1.3 NA Plan-Neofluar oil-immersion objective and a thermostatically regulated chamber (Pecon, Erbach, Germany) at 37 °C in a humidified atmosphere of 5% CO_2/95% air. Cells were maintained at 20% O_2 for 10 min to allow for equilibration and then reduced to 5% O_2 using the equipment described above. After 60 min of equilibration the cells were exposed to NaN_3 (0.2 mg/ml) or AA (10 μM). TMRM and MM2 probe fluorescence intensities were recorded. Experiments were terminated by addition of D-(+)-Glucose (100 mM) and glucose oxidase (100 μg/ml) to completely deplete the available oxygen. In another set of experiments, Hela cells were maintained at 20% O_2. After a 10-min equilibration period, cells were exposed to sodium azide (NaN_3, 0.2 mg/ml) or AA (10 μM) and TMRM and MM2 probe intensity ratio was recorded as described above.

Induction of apoptosis and simultaneous measurement of oxygen consumption and GFP redistribution. HeLa cyt-*c*-GFP cells were cultured in glass bottom dishes and incubated with 10 μg/ml MM2 probe for 16 h followed by TMRM (30 nM) and zVAD-fmk (100 μM) for 30 min to inhibit caspase activation. After treatment with STS, caspase activation would otherwise trigger mitochondrial demise following MOMP due to cleavage of complex I.[9,11,30] Cells were mounted on stage as described above and maintained in 20% O_2 for the required 10 min of equilibration. Then O_2 was reduced to 2% using the equipment described above. After 60 min cells were treated with 3 μM STS. During the subsequent time lapse imaging experiments, glucose was added to the medium as indicated. All images were processed using ImageJ (1.45) and MetaMorph Software version 7.5 as described above. The distribution of cyt-*c*-GFP was calculated using the S.D. of the average pixel intensity as described previously.[31] A decrease in the S.D. value indicates the redistribution of GFP from punctate (mitochondrial) to homogeneous (cytoplasm and nucleus) patterns. For further analysis of cell responses, cells were grouped into three classes based on their intracellular O_2 kinetics following MOMP: (a) Cells with an increase in intracellular O_2 following MOMP (the average of the 10 upstream values+S.D. was smaller than the average of the 10 downstream values following MOMP). (b) Cells with a decrease in intracellular O_2 following MOMP (the average of the 10 upstream values+S.D. was larger than the average of the 10 downstream values following MOMP). (c) Cells with no change in intracellular O_2 following MOMP (remainder of cells).

Statistics. Data are given as means ± S.E.M. For statistical comparison, one-way analysis of variance, paired samples *t*-test, Wilcoxon test and Friedman's test were carried out using SPSS software (SPSS version 23, IBM). Where the *p*-value was < 0.05, groups were considered to be significantly different. All experiments were carried out in triplicate unless indicated otherwise.

Conflict of Interest

D.P. is a stakeholder of Luxcel Biosciences, a company which produces the oxygen sensor used in this study. The other authors have no conflict of interest.

Acknowledgements. We thank James Kealey for advice on the manuscript. This research was supported by grants from Science Foundation Ireland (13/IA/1881) and the European Union FP7 Marie Curie IAPP program (OXY-SENSE; Contract 230641) to J.H.M.P.

1. Semenza GL. Life with oxygen. *Science* 2007; **318**: 62–64.
2. Banasiak KJ, Xia Y, Haddad GG. Mechanisms underlying hypoxia-induced neuronal apoptosis. *Prog Neurobiol* 2000; **62**: 215–249.
3. Hockel M, Schlenger K, Aral B, Mitze M, Schaffer U, Vaupel P. Association between tumor hypoxia and malignant progression in advanced cancer of the uterine cervix. *Cancer Res* 1996; **56**: 4509–4515.
4. Vaupel P, Mayer A. Hypoxia in cancer: significance and impact on clinical outcome. *Cancer Metastasis Rev* 2007; **26**: 225–239.
5. Adachi S, Gottlieb RA, Babior BM. Lack of release of cytochrome C from mitochondria into cytosol early in the course of Fas-mediated apoptosis of Jurkat cells. *J Biol Chem* 1998; **273**: 19892–19894.
6. Cai J, Jones DP. Superoxide in apoptosis. Mitochondrial generation triggered by cytochrome c loss. *J Biol Chem* 1998; **273**: 11401–11404.
7. Mootha VK, Wei MC, Buttle KF, Scorrano L, Panoutsakopoulou V, Mannella CA *et al.* A reversible component of mitochondrial respiratory dysfunction in apoptosis can be rescued by exogenous cytochrome c. *EMBO J* 2001; **20**: 661–671.
8. Tamm I, Kornblau SM, Segall H, Krajewski S, Welsh K, Kitada S *et al.* Expression and prognostic significance of IAP-family genes in human cancers and myeloid leukemias. *Clin Cancer Res* 2000; **6**: 1796–1803.
9. Huber HJ, Dussmann H, Kilbride SM, Rehm M, Prehn JH. Glucose metabolism determines resistance of cancer cells to bioenergetic crisis after cytochrome-c release. *Mol Syst Biol* 2011; **7**: 470.
10. Tait SW, Parsons MJ, Llambi F, Bouchier-Hayes L, Connell S, Munoz-Pinedo C *et al.* Resistance to caspase-independent cell death requires persistence of intact mitochondria. *Dev Cell* 2010; **18**: 802–813.
11. Waterhouse NJ, Goldstein JC, von Ahsen O, Schuler M, Newmeyer DD, Green DR. Cytochrome c maintains mitochondrial transmembrane potential and ATP generation after outer mitochondrial membrane permeabilization during the apoptotic process. *J Cell Biol* 2001; **153**: 319–328.
12. Quaegebeur A, Carmeliet P. Oxygen sensing: a common crossroad in cancer and neurodegeneration. *Curr Top Microbiol Immunol* 2010; **345**: 71–103.
13. Papkovsky DB, Dmitriev RI. Biological detection by optical oxygen sensing. *Chem Soc Rev* 2013; **42**: 8700–8732.
14. Springett R, Swartz HM. Measurements of oxygen *in vivo*: overview and perspectives on methods to measure oxygen within cells and tissues. *Antioxid Redox Signal* 2007; **9**: 1295–1301.
15. Dunphy I, Vinogradov SA, Wilson DF. Oxyphor R2 and G2: phosphors for measuring oxygen by oxygen-dependent quenching of phosphorescence. *Anal Biochem* 2002; **310**: 191–198.
16. Esipova TV, Karagodov A, Miller J, Wilson DF, Busch TM, Vinogradov SA. Two new "protected" oxyphors for biological oximetry: properties and application in tumor imaging. *Anal Chem* 2011; **83**: 8756–8765.
17. Dmitriev RI, Zhdanov AV, Jasionek G, Papkovsky DB. Assessment of cellular oxygen gradients with a panel of phosphorescent oxygen-sensitive probes. *Anal Chem* 2012; **84**: 2930–2938.
18. Whalen WJ, Riley J, Nair P. A microelectrode for measuring intracellular PO2. *J Appl Physiol* 1967; **23**: 798–801.
19. Gleichmann M, Collis LP, Smith PJ, Mattson MP. Simultaneous single neuron recording of O2 consumption, [Ca2+]i and mitochondrial membrane potential in glutamate toxicity. *J Neurochem* 2009; **109**: 644–655.
20. Liu Y, Villamena FA, Sun J, Wang TY, Zweier JL. Esterified trityl radicals as intracellular oxygen probes. *Free Radic Biol Med* 2009; **46**: 876–883.
21. Wu CC, Luk HN, Lin YT, Yuan CY. A Clark-type oxygen chip for *in situ* estimation of the respiratory activity of adhering cells. *Talanta* 2010; **81**: 228–234.
22. Sakadzic S, Roussakis E, Yaseen MA, Mandeville ET, Srinivasan VJ, Arai K *et al.* Two-photon high-resolution measurement of partial pressure of oxygen in cerebral vasculature and tissue. *Nat Methods* 2010; **7**: 755–759.

23. Ji J, Rosenzweig N, Jones I, Rosenzweig Z. Molecular oxygen-sensitive fluorescent lipobeads for intracellular oxygen measurements in murine macrophages. *Anal Chem* 2001; **73**: 3521–3527.
24. Wilson DF. Quantifying the role of oxygen pressure in tissue function. *Am J Physiol Heart Circ Physiol* 2008; **294**: H11–H13.
25. Kondrashina AV, Dmitriev RI, Borisov SM, Klimant I, O'Brian I, Nolan YM *et al.* A phosphorescent nanoparticle based probe for sensing and imaging of (intra)cellular oxygen in multiple detection modalities. *Adv Function Mater* 2012; **22**: 4931–4939.
26. Carreau A, El Hafny-Rahbi B, Matejuk A, Grillon C, Kieda C. Why is the partial oxygen pressure of human tissues a crucial parameter? Small molecules and hypoxia. *J Cell Mol Med* 2011; **15**: 1239–1253.
27. Fercher A, Borisov SM, Zhdanov AV, Klimant I, Papkovsky DB. Intracellular O2 sensing probe based on cell-penetrating phosphorescent nanoparticles. *ACSnano* 2011; **5**: 10.
28. Lesniak A, Campbell A, Monopoli MP, Lynch I, Salvati A, Dawson KA. Serum heat inactivation affects protein corona composition and nanoparticle uptake. *Biomaterials* 2010; **31**: 9511–9518.
29. Rossignol R, Gilkerson R, Aggeler R, Yamagata K, Remington SJ, Capaldi RA. Energy substrate modulates mitochondrial structure and oxidative capacity in cancer cells. *Cancer Res* 2004; **64**: 985–993.
30. Ricci JE, Gottlieb RA, Green DR. Caspase-mediated loss of mitochondrial function and generation of reactive oxygen species during apoptosis. *J Cell Biol* 2003; **160**: 65–75.
31. Dussmann H, Rehm M, Kogel D, Prehn JH. Outer mitochondrial membrane permeabilization during apoptosis triggers caspase-independent mitochondrial and caspase-dependent plasma membrane potential depolarization: a single-cell analysis. *J Cell Sci* 2003; **116**(Pt 3): 525–536.
32. O'Riordan TC, Fitzgerald K, Ponomarev GV, Mackrill J, Hynes J, Taylor C *et al.* Sensing intracellular oxygen using near-infrared phosphorescent probes and live-cell fluorescence imaging. *Am J Physiol Regul Integr Comp Physiol* 2007; **292**: R1613–R1620.
33. Ward JP. Oxygen sensors in context. *Biochim Biophys Acta* 2008; **1777**: 1–14.
34. Jekabsons MB, Nicholls DG. *In situ* respiration and bioenergetic status of mitochondria in primary cerebellar granule neuronal cultures exposed continuously to glutamate. *J Biol Chem* 2004; **279**: 32989–33000.
35. Wu M, Neilson A, Swift AL, Moran R, Tamagnine J, Parslow D *et al.* Multiparameter metabolic analysis reveals a close link between attenuated mitochondrial bioenergetic function and enhanced glycolysis dependency in human tumor cells. *Am J Physiol Cell Physiol* 2007; **292**: C125–C136.
36. Eidi H, Joubert O, Nemos C, Grandemange S, Mograbi B, Foliguet B *et al.* Drug delivery by polymeric nanoparticles induces autophagy in macrophages. *Int J Pharm* 2012; **422**: 495–503.
37. Zhdanov AV, Favre C, O'Flaherty L, Adam J, O'Connor R, Pollard PJ *et al.* Comparative bioenergetic assessment of transformed cells using a cell energy budget platform. *Integr Biol (Camb)* 2011; **3**: 1135–1142.
38. Pacheco-Torres J, Lopez-Larrubia P, Ballesteros P, Cerdan S. Imaging tumor hypoxia by magnetic resonance methods. *NMR Biomed* 2010; **24**: 1–16.
39. Flanagan L, Sebastia J, Tuffy LP, Spring A, Lichawska A, Devocelle M *et al.* XIAP impairs Smac release from the mitochondria during apoptosis. *Cell Death Dis* 2010; **1**: e49.
40. Kilbride SM, Prehn JH. Central roles of apoptotic proteins in mitochondrial function. *Oncogene* 2013; **32**: 2703–2711.
41. Ward MW, Concannon CG, Whyte J, Walsh CM, Corley B, Prehn JH. The amyloid precursor protein intracellular domain(AICD) disrupts actin dynamics and mitochondrial bioenergetics. *J Neurochem* 2010; **113**: 275–284.
42. Aragones J, Fraisl P, Baes M, Carmeliet P. Oxygen sensors at the crossroad of metabolism. *Cell Metab* 2009; **9**: 11–22.
43. Chandel NS, Schumacker PT. Cellular oxygen sensing by mitochondria: old questions, new insight. *J Appl Physiol (1985)* 2000; **88**: 1880–1889.
44. Guzy RD, Schumacker PT. Oxygen sensing by mitochondria at complex III: the paradox of increased reactive oxygen species during hypoxia. *Exp Physiol* 2006; **91**: 807–819.
45. Rumsey WL, Schlosser C, Nuutinen EM, Robiolio M, Wilson DF. Cellular energetics and the oxygen dependence of respiration in cardiac myocytes isolated from adult rat. *J Biol Chem* 1990; **265**: 15392–15402.
46. Wilson DF, Erecinska M. The oxygen dependence of cellular energy metabolism. *Adv Exp Med Biol* 1986; **194**: 229–239.
47. Xu RH, Pelicano H, Zhou Y, Carew JS, Feng L, Bhalla KN *et al.* Inhibition of glycolysis in cancer cells: a novel strategy to overcome drug resistance associated with mitochondrial respiratory defect and hypoxia. *Cancer Res* 2005; **65**: 613–621.
48. Zu XL, Guppy M. Cancer metabolism: facts, fantasy, and fiction. *Biochem Biophys Res Commun* 2004; **313**: 459–465.
49. Saraste M. Oxidative phosphorylation at the fin de siecle. *Science* 1999; **283**: 1488–1493.
50. Nicholls DG, Ward MW. Mitochondrial membrane potential and neuronal glutamate excitotoxicity: mortality and millivolts. *Trends Neurosci* 2000; **23**: 166–174.
51. Hagen T, Taylor CT, Lam F, Moncada S. Redistribution of intracellular oxygen in hypoxia by nitric oxide: effect on HIF1alpha. *Science* 2003; **302**: 1975–1978.
52. Thienpont B, Steinbacher J, Zhao H, D'Anna F, Kuchnio A, Ploumakis A *et al.* Tumour hypoxia causes DNA hypermethylation by reducing TET activity. *Nature* 2016; **537**: 63–68.
53. Rehm M, Dussmann H, Prehn JH. Real-time single cell analysis of Smac/DIABLO release during apoptosis. *J Cell Biol* 2003; **162**: 1031–1043.
54. Rehm M, Huber HJ, Hellwig CT, Anguissola S, Dussmann H, Prehn JH. Dynamics of outer mitochondrial membrane permeabilization during apoptosis. *Cell Death Differ* 2009; **16**: 613–623.